ELSEVIER

Bioelectrochemistry 57 (2002) 83–87

Bioelectrochemistry

www.elsevier.com/locate/bioelechem

Calculation of dielectric spectra of suspensions of rod-shaped cells using boundary element method

Katsuhisa Sekine [a,*], Nobue Torii [a], Chihiro Kuroda [a], Koji Asami [b]

[a]School of Health Sciences, Faculty of Medicine, Kanazawa University, 5-11-80 Kodatsuno, Kanazawa 920-0942, Japan
[b]Institute for Chemical Research, Kyoto University, Uji, Kyoto 611-0011, Japan

Received 2 May 2001; received in revised form 13 November 2001; accepted 10 December 2001

Abstract

The boundary element method (BEM) has been applied to the calculation of dielectric spectra of suspensions of rod-shaped cells using two kinds of models: model-R consisting of a cylinder and two hemispheres and model-PU of prolate spheroid shape. Both models have an insulating shell phase of a uniform thickness. The calculations were compared with those using a conventional spheroidal model with a confocal shell (model-PC) and previous observations on rod-shaped yeast cells. The differences among the three models were not considerable and all the models succeeded in interpreting the observed data on yeast cells.

Keywords: Boundary element method; Complex permittivity; Dielectric relaxation; Interfacial polarization; Simulation

1. Introduction

Biological cell suspensions show dielectric relaxation due to interfacial polarization in the radio-frequency region [1–4]. Since the dielectric relaxation of this kind is sensitive to cell shape, dielectric spectroscopy is effective in detecting changes in cell shape in situ, such as those of yeast cells with the growth [5–8] and of erythrocytes under high pressures [9].

To assess the effects of cell shape on the dielectric relaxation, an ellipsoidal cell model with a confocal shell has been used [5,7,10–12]. These cell models, however, cannot necessarily represent real shape of cells and do not meet uniformity of thickness of the plasma membrane. These discrepancies between cells and their models depress reliability of the theoretical analyses. Recently, we developed a method for calculating dielectric spectra of suspensions using the boundary element method (BEM) [13,14]. The calculations showed that the dielectric spectra for cell models in the shape of doublet and biconcave could not be imitated by the conventional spheroidal models [13], and that the nonuniformity of the thickness of the shell phase in w/o/w emulsions altered the dielectric spectra [14]. These situations mean that theoretical calculations based on realistic cell models are needed for reliable analyses of dielectric spectra. In the present study, theoretical calculations are made by the BEM method to reexamine the dielectric spectra of the suspensions of rod-shaped yeast cells that were studied previously [7].

2. Models and method of calculation

2.1. Cell models

Biological cells that the cytoplasm is covered with the plasma membrane may be represented by shelled models consisting of an inner phase and a shell phase [1–4]. To examine the effects of the cell shape and the uniformity of the membrane thickness, we used three models R, PU, and PC with diameter D and length L, as shown in Fig. 1. Model-R is of rod shape with a cylinder of diameter D and length $L-D$, and two hemispheres of diameter D. Model-PU is a prolate spheroid characterized by semiaxes $D/2$ in xy-plane and $L/2$ along z-axis. The thickness T of the shell phase of model-R and -PU is made uniform. Model-PC, which has been used in conventional theoretical calculations [10–12], consists of two confocal prolate spheroids, the outer one being the same as the outer surface of model-PU and the inner one being characterized by semiaxes [(D/

* Corresponding author. Tel.: +81-76-265-2586; fax: +81-76-234-4360.
E-mail address: sekine@kenroku.kanazawa-u.ac.jp (K. Sekine).

1567-5394/02/$ - see front matter
PII: S1567-5394(02)00002-6

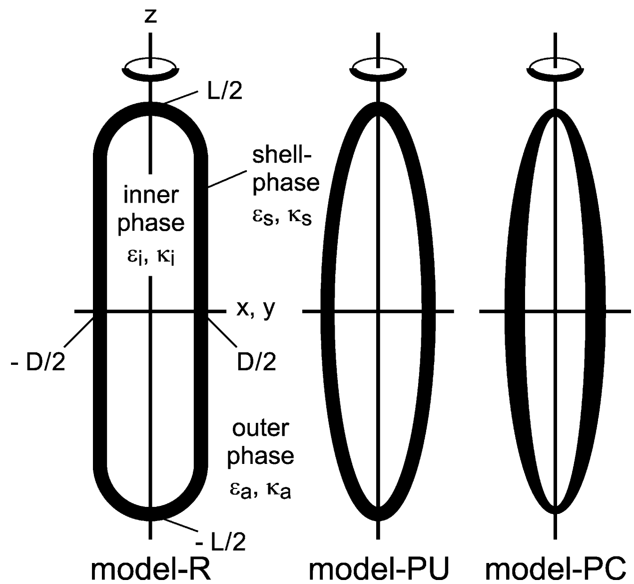

Fig. 1. Models for rod-shaped cells.

$2)^2-K]^{1/2}$ and $[(L/2)^2-K]^{1/2}$, where K is a parameter representing a family of the confocal surfaces. The shell phase is the region between these two spheroidal surfaces and, therefore, its thickness is not uniform.

2.2. Method of calculation

Because of $D_{\infty h}$ symmetry of the model particles, the complex permittivity ε^* of their suspension can be represented by the following relations when the particles are randomly oriented [13,14]:

$$\frac{\varepsilon^* - \varepsilon_a^*}{\varepsilon^* + 2\varepsilon_a^*} = \frac{P}{9}(2\beta_h + \beta_z), \tag{1}$$

where ε_a^* is the complex permittivity of the outer phase, P the volume fraction of the suspension, β_k (k=h, z) the polarization coefficient for the particle defined by $\beta_k = \alpha_k/(V\varepsilon_a^*)$, α_k the polarizability, and V the volume of the particle, subscripts h and z denoting the directions in xy-plane and along z-axis, respectively. The complex permittivities are defined by $\varepsilon^* = \varepsilon + \kappa/(i\omega\varepsilon_0)$ with relative permittivity ε, electrical conductivity κ, an imaginary unit i, angular frequency ω represented by $\omega = 2\pi f$ in terms of frequency f, and the permittivity of vacuum ε_0.

When $P \ll 1$, Eq. (1) becomes [5]

$$\varepsilon_D^* = \varepsilon_D + \kappa_D/(i\omega\varepsilon_0) \equiv (\varepsilon^* - \varepsilon_a^*)/P = 2\varepsilon_{D_h}^* + \varepsilon_{D_z}^*, \tag{2}$$

where

$$\varepsilon_{D_k}^* = \varepsilon_{D_k} + \kappa_{D_k}/(i\omega\varepsilon_0) = \varepsilon_a^*\beta_k/3. \tag{3}$$

This equation was used for assessing the effects of the cell shape and the thickness uniformity on the dielectric spectra. The calculations of β_k at frequencies from 1 to 10^{10} Hz were made for model-R and -PU using BEM [13] and for model-PC using analytical equations [10].

Table 1 shows the parameter values used in the calculations. The values of D and L were chosen so as to imitate the size of the yeast cells used in the previous experimental study [7], T being typical of biological cells [15,6]. The value of κ_a of the outer phase was comparable with that of a 30 mM KCl solution [16] used in the experimental study. To focus the attention on the effects of the cell shape and the uniformity of the membrane thickness, ε_s, κ_s of the shell phase and ε_i, κ_i of the inner phase were assumed to be independent of frequency, by neglecting their slight frequency-dependent behavior [1,2]. The value of ε_s was chosen so that the membrane capacitance per unit area ($\varepsilon_s\varepsilon_0/T$) was 0.7 μF cm^{-2}, which was typical of cell membranes [1,2,5]. The values of ε_i and κ_i were made to be the same as ε_a and κ_a for simplicity. Values of K in model-PC were made so that the volume of the inner phase was the same as that of model-PU, namely,

$$[(D/2)^2 - K][(L/2)^2 - K]^{1/2} = [(D/2) - T]^2[(L/2) - T]. \tag{4}$$

Table 1
Parameter values used in calculations of dielectric spectra

Size of model-particles		
Diameter, D	4.1 μm	
Length, L	from $2 \times D$ to $14 \times D$	
Thickness of shell phase, T	7.0 nm	
Relative permittivity ε and conductivity κ of phases		
Outer phase	ε_a=80	κ_a=0.27 S m^{-1}
Shell phase	ε_s=5.53	κ_s=0
Inner phase	ε_i=80	κ_i=0.27 S m^{-1}

Table 2
Values of ε_D^* (relative permittivity ε_D and conductivity κ_D) evaluated with BEM using different meshes that have different numbers of elements NE and nodes NN

NE	NN	10 Hz		100 kHz		1 GHz	
		10^{-4} ε_D	10 κ_D/(S m^{-1})	10^{-3} ε_D	10 κ_D/(S m^{-1})	ε_D	10^2 κ_D/(S m^{-1})
Model-R (q=14)							
160	722	7.778	−4.444	7.341	−3.670	−2.615	−1.751
224	1010	7.778	−4.443	7.339	−3.674	−2.617	−1.752
312	1406	7.778	−4.443	7.338	−3.674	−2.616	−1.752
Model-PU (q=14)							
160	722	6.797	−4.470	7.514	−3.621	−2.998	−2.003
192	866	6.795	−4.469	7.522	−3.619	−3.001	−2.003
312	1406	6.795	−4.467	7.517	−3.618	−3.000	−2.003

3. Results and discussion

3.1. Accuracy of BEM calculations

Since the accuracy in BEM calculations depends on how to divide the boundary into elements, we examined three different meshes in the cases of model-R and -PU with the axial ratio q (=L/D) of 14. The calculations of ε_D^* provided the same results with four significant figures (Table 2). This indicates that the mesh size used was small enough to attain sufficient accuracy.

3.2. Behavior of β_k

Fig. 2(A) shows frequency dependence of the real (β_k') and the imaginary (β_k'') parts of β_k (=$\beta_k' + i\beta_k''$) for model-R with q of 14. As seen from this figure, β_h shows a one-step relaxation denoted by h1R. On the other hand, β_z consists of

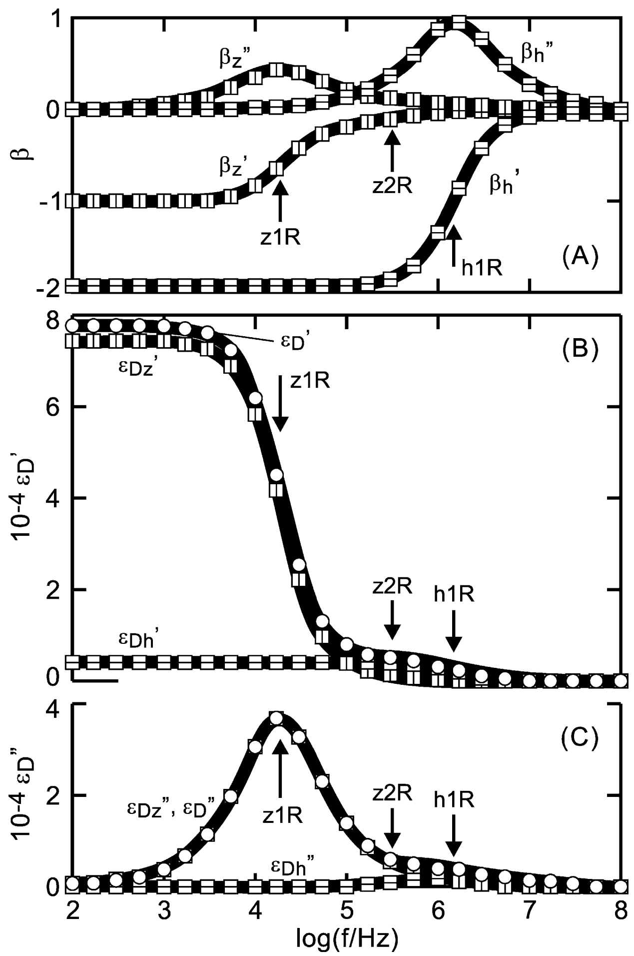

Fig. 2. Frequency-dependence of (A) polarization coefficients β_h, β_z (real parts β_h', β_z' and imaginary parts β_h'', β_z''), (B) real (ε_{D_h}', ε_{D_z}', ε_D'), and (C) imaginary (ε_{D_h}'', ε_{D_z}'', ε_D'') parts of complex permittivities $\varepsilon_{D_h}^*$, $\varepsilon_{D_z}^*$, and ε_D^* for model-R with the axial ratio q of 14. Subscripts h and z denote the directions in xy-plane and along z-axis, respectively. Values of ε_{D_h}'', ε_{D_z}'', and ε_D'' were obtained by subtracting the limiting values (L_h^e, L_z^e, L^e) of the conductivities (κ_{D_h}, κ_{D_z}, κ_D) at low frequencies, as $\varepsilon_D'' = (\kappa_D - L^e)/(\omega\varepsilon_0)$.

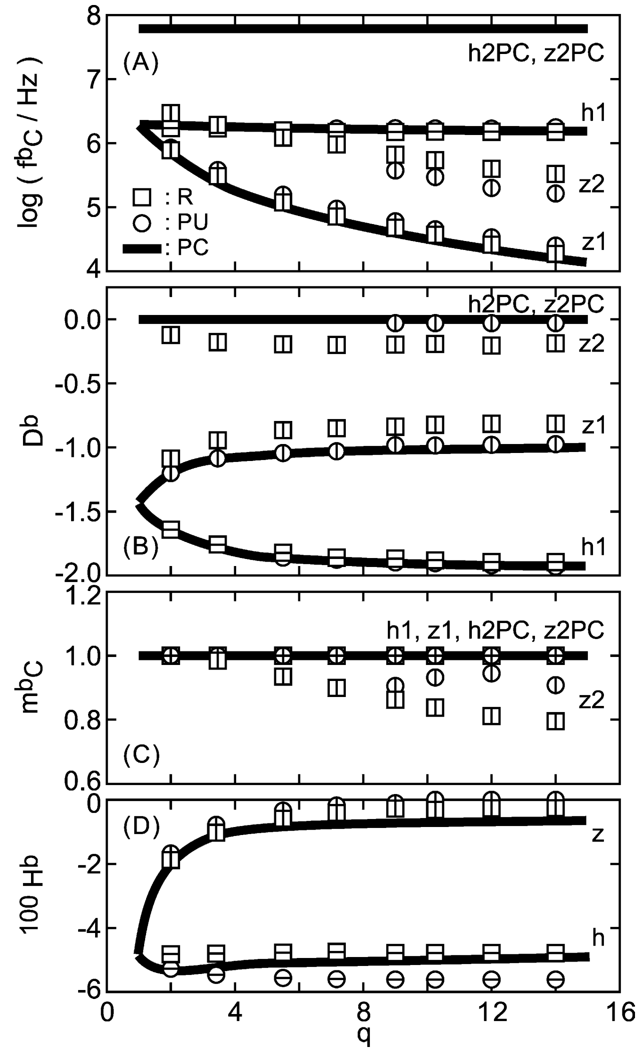

Fig. 3. Change in relaxation parameters for β with q. (A) The characteristic frequency f_C^b, (B) the relaxation intensity D^b, (C) the Cole–Cole parameter m_C^b, and (D) the limiting value H^b at high frequencies.

two relaxation terms, z1R and z2R. To obtain dielectric relaxation parameters for these relaxation terms, we assumed the Cole–Cole type relaxation [17], i.e., $D^b/[1+(i\omega\tau_C^b)^{m_C^b}]$, where D^b is the relaxation intensity, τ_C^b the relaxation time and m_C^b the Cole–Cole parameter. Fig. 3 shows the values of the characteristic frequency f_C^b (=$1/(2\pi\tau_C^b)$), D^b, m_C^b and the limiting value H^b of β_k at high frequencies.

As shown in Fig. 3, β_h and β_z for model-R consisted of one (h1R) and two (z1R and z2R) relaxation terms, respectively, irrespective of q. In the case of model-PU, similar relaxation terms were found in β_h (h1PU) and β_z (z1PU and z2PU) when $q \geq 9.0$. In case $q \leq 7.1$, it was difficult to differentiate z2PU from z1PU, because D^b of z2PU was much lower than that of z1PU, as seen in Fig. 3(B). Both β_h and β_z for model-PC consisted of two relaxation terms, which were denoted by h1PC and z1PC for the low-frequency terms, and h2PC and z2PC for the high-frequency ones.

The relaxation terms can be classified into four types based on the values of f_C^b shown in Fig. 3(A). Type-h1 contains h1R, h1PU, and h1PC located near 2 MHz independent of q. Type-z1 contains z1R, z1PU, and z1PC shifting to lower frequencies with the increase in q. Based on conventional theoretical considerations [5,7], type-h1 and -z1, respectively, can be related to the shape of the particles in xy-plane and along z-axis. Type-2PC (h2PC and z2PC) can be distinguished from type-z2 (z2R and z2PU) by its much higher $f_C{}^b$, being considered to be related to the inner phase and not to be found in model-R and -PU because of its very low intensity. The relaxation mechanism for type-z2 is not made clear at this stage.

3.3. Behavior of ε_{D_k}* and ε_D*

Fig. 2(B) and (C), respectively, show the frequency dependence of the real and the imaginary parts of ε_{D_k}* and ε_D* for model-R with q of 14. As seen from the figures, the frequency dependence of ε_D* can be represented as a two-step relaxation consisting of z1R and h1R, because z2R is hidden in the tails of these terms. This two-step relaxation found in ε_D* is consistent with the experimental observations on rod-shaped yeast cells [7].

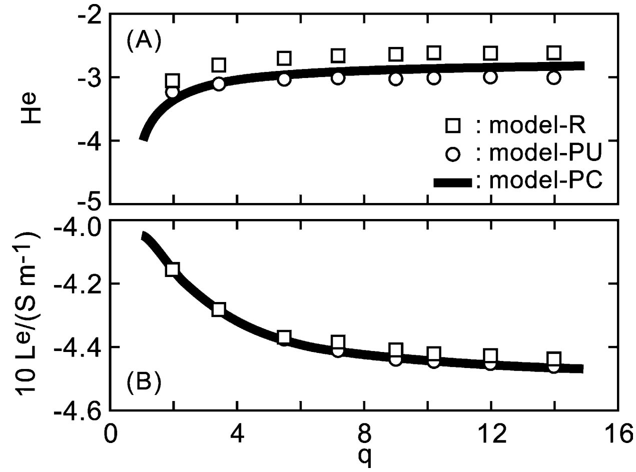

Fig. 5. Change in relaxation parameters for ε_D* with q. (A) The limiting value of ε_D at high frequencies H^e and (B) that of κ_D at low frequencies L^e.

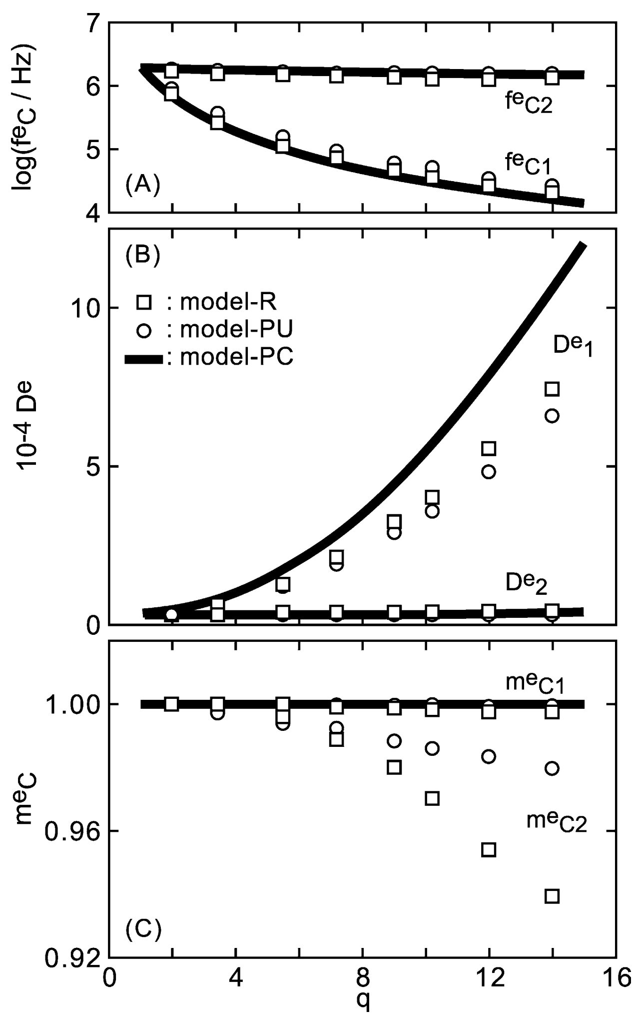

Fig. 4. Change in relaxation parameters for ε_D* with q. (A) The characteristic frequency f_C^e, (B) the relaxation intensity D^e, and (C) the Cole–Cole parameter m_C^e.

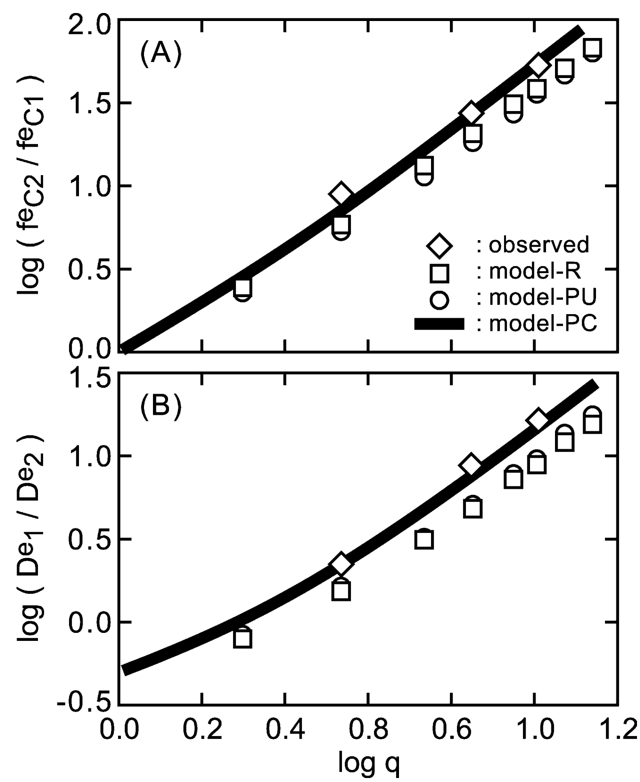

Fig. 6. Change in ratios (A) $f_{C_2}^e/f_{C_1}^e$ and (B) D_1^e/D_2^e with q. The standard error of the observed data is less than the size of the mark.

To perform practical analysis of the frequency dependence of $\varepsilon_D{}^*$, $\varepsilon_D{}^*$ was expressed by a sum of two relaxation terms of the Cole–Cole type [17] as

$$\varepsilon_D{}^* = H^e + \frac{D_1^e}{1+(i\omega\tau_{C_1}^e)^{m_{C_1}^e}} + \frac{D_2^e}{1+(i\omega\tau_{C_2}^e)^{m_{C_2}^e}} + \frac{L^e}{i\omega\varepsilon_0}, \tag{5}$$

where H^e is the limiting value of ε_D at high frequencies, L^e that of κ_D at low frequencies, D^e the relaxation intensity, τ_C^e the relaxation time and m_C^e the Cole–Cole parameter. Subscripts 1 and 2 denote the low- and the high-frequency relaxation, respectively. Figs. 4 and 5 show the change in these relaxation parameters with q. The characteristic frequencies $f_{C_1}^e$ and $f_{C_2}^e$ in Fig. 4(A) were obtained from $\tau_{C_1}^e$ and $\tau_{C_2}^e$, respectively. Fig. 6 shows the plots of the ratios $f_{C_2}^e/f_{C_1}^e$ and D_1^e/D_2^e against q.

It is seen from Figs. 4–6 that neither of the shape of the model and the uniformity of the shell-thickness produces significant effects on the dielectric spectra of the suspensions. The behavior of the ratios $f_{C_2}^e/f_{C_1}^e$ and D_1^e/D_2^e for the measured data [7] can be quantitatively explained using all of the models. A remaining subject to be investigated in future studies is how to deal with the distribution of cell size, which is commonly found in cell populations used in experimental studies. A value of 0.9 obtained for $m_{C_1}^e$ and $m_{C_2}^e$ from the experimental data [7] could be due to the distribution of cell size. For quantitative examinations of its effects, modifications of the calculation method are necessary.

References

[1] R. Pethig, D.B. Kell, The passive electrical properties of biological systems: their significance in physiology, biophysics, and biotechnology, Phys. Med. Biol. 32 (1987) 933–970.

[2] S. Takashima, Electrical Properties of Biopolymers and Membranes, Adam Hilger, Bristol, 1989.

[3] K. Asami, Dielectric relaxation spectroscopy of biological cell suspensions, in: V.A. Hackley, J. Texter (Eds.), Handbook on Ultrasonic and Dielectric Characterization Techniques for Suspended Particulates, The American Ceramic Society, Westerville, 1998, pp. 333–349.

[4] K.R. Foster, H.P. Schwan, Dielectric properties of tissues, in: C. Polk, E. Postow (Eds.), Handbook of Biological Effects of Electromagnetic Fields, 2nd edn., CRC Press, Boca Raton, FL, 1996, pp. 25–102.

[5] K. Asami, T. Yonezawa, Dielectric behavior of nonspherical cells in culture, Biochim. Biophys. Acta 1245 (1995) 317–324.

[6] K. Asami, E. Gheorghiu, T. Yonezawa, Dielectric behavior of budding yeast in cell separation, Biochim. Biophys. Acta 1381 (1998) 234–240.

[7] K. Asami, Effect of cell shape on dielectric behavior of fission yeast, Biochim. Biophys. Acta 1472 (1999) 137–141.

[8] K. Asami, E. Gheorghiu, T. Yonezawa, Real-time monitoring of yeast cell division by dielectric spectroscopy, Biophys. J. 76 (1999) 3345–3348.

[9] K. Asami, T. Yamaguchi, Electrical and morphological changes of human erythrocytes under high hydrostatic pressure followed by dielectric spectroscopy, Ann. Biomed. Eng. 27 (1999) 427–435.

[10] K. Asami, T. Hanai, N. Koizumi, Dielectric approach to suspensions of ellipsoidal particles covered with a shell in particular reference to biological cells, Jpn. J. Appl. Phys. 19 (1980) 359–365.

[11] P. Gascoyne, R. Pethig, J. Satayavivad, F.F. Becker, M. Ruchirawat, Dielectrophoretic detection of changes in erythrocyte membranes following malarial infection, Biochim. Biophys. Acta 1323 (1997) 240–252.

[12] R.D. Miller, T.B. Jones, Electro-orientation of ellipsoidal erythrocytes: theory and experiment, Biophys. J. 64 (1993) 1588–1595.

[13] K. Sekine, Application of boundary element method to calculation of the complex permittivity of suspensions of cells in shape of $D_{\infty h}$ symmetry, Bioelectrochemistry 52 (2000) 1–7.

[14] K. Sekine, C. Kuroda, N. Torii, Boundary-element calculations for dielectric relaxation of water-in-oil-in-water emulsions consisting of spherical droplets with a spheroidal core, Colloid Polym. Sci. 280 (2002) 71–77.

[15] L. Stryer, Biochemistry, 4th edn., Freeman, New York, 1995.

[16] P. Vanýsek, Equivalent conductivity of electrolytes in aqueous solution, in: D.R. Lide (Ed.), CRC Handbook of Chemistry and Physics, 79th edn., CRC Press, Boca Raton, FL, 1998, p. 92.

[17] K.S. Cole, R.H. Cole, Dispersion and absorption in dielectrics, J. Chem. Phys. 9 (1941) 341–351.